Antimicrobial Bilayer Nanocomposites Based on the Incorporation of As-Synthetized Hollow Zinc Oxide Nanotubes

Carol López de Dicastillo [1,2,*], **Cristian Patiño Vidal [1,2]**, **Irene Falcó [3]**, **Gloria Sánchez [3]**, **Paulina Márquez [2,4] and Juan Escrig [2,4]**

[1] Center of Innovation in Packaging (LABEN), Department of Food Science and Technology, Technology Faculty, University of Santiago de Chile (USACH), Santiago 9170201, Chile; cristian.patino@usach.cl

[2] CEDENNA (Center for the Development of Nanoscience and Nanotechnology), Santiago 9170124, Chile; paulina.marquez.m@usach.cl (P.M.); juan.escrig@usach.cl (J.E.)

[3] Department of Preservation and Food Safety Technologies, Institute of Agrochemistry and Food technology (IATA-CSIC), 46980 Paterna, Valencia, Spain; iff26388@hotmail.es (I.F.); gloriasanchez@iata.csic.es (G.S.)

[4] Department of Physics, University of Santiago de Chile (USACH), Santiago 9170124, Chile

* Correspondence: analopez.dediscastillo@usach.cl

Abstract: An antimicrobial polymeric bilayer structure based on the application of an acrylic coating containing hollow zinc oxide nanotubes over a polymeric substrate was developed in this work. Firstly, zinc oxide nanotubes (ZnO_{NT}) were obtained by an atomic layer deposition (ALD) process over electrospun polyvinyl alcohol nanofibers followed by polymer removal through calcination with the purpose of obtaining antimicrobial nanostructures with a high specific area. Parameters of electrospinning, ALD, and calcination processes were set in order to obtain successfully hollow zinc oxide nanotubes. Morphological studies through scanning electron microscopy (SEM) and transmission electron microscopy (TEM) microscopies confirmed the morphological structure of ZnO_{NT} with an average diameter of 180 nm and thickness of approximately 60 nm. Thermal and X-ray diffraction (XRD) analyses provided evidence that calcination completely removed the polymer, resulting in a crystalline hexagonal wurtzite structure. Subsequently, ZnO_{NT} were incorporated into a polymeric coating over a polyethylene extruded film at two concentrations: 0.5 and 1 wt. % with respect to the polymer weight. An antimicrobial analysis of developed antimicrobial materials was performed following JIS Z2801 against *Staphylococcus aureus* and *Escherichia coli.* When compared to active materials containing commercial ZnO nanoparticles, materials containing ZnO_{NT} presented higher microbial inhibition principally against Gram-negative bacteria, whose reduction was total for films containing 1 wt. % ZnO_{NT}. Antiviral studies were also performed, but these materials did not present significant viral reduction.

Keywords: atomic layer deposition; electrospinning; nanotube; zinc oxide

1. Introduction

Nowadays, the interest toward antimicrobial materials, such as antimicrobial packaging, surfaces, and paintings, has increased due to the high incidence of nosocomial diseases, hospital infections, and the increase of microbial resistance. Several developments based on the incorporation of antimicrobial substances into polymeric matrixes have been carried out in order to reduce and inhibit microbial presence [1,2]. Specifically, the research focused on novel antimicrobial nanocomposites whose activities are related to antimicrobial nanoparticles (NPs) has increased over last years since

antimicrobial nanostructures are one of the most promising alternatives in the search for new antimicrobial substances [3–5]. The attention has been principally centered on metallic/metal oxide nanoparticles due to their broad antibacterial and antifungal activities at low concentrations thanks to their high specific area [6–9].

Zinc oxide (ZnO) nanoparticles are an inorganic material with optical, chemical sensing, electric conductivity, catalytic, photochemical, and antimicrobial properties. This metal oxide presents three crystal structures: wurtzite, zinc blend, and rocksalt, with a direct wide band gap of 3.3 Ev [10]. Some works have evidenced ZnO nanoparticles with dimensions smaller than 100 nm have shown increasing antimicrobial properties against Gram-negative and Gram-positive bacteria due to a higher cellular internalization. Specifically, Verma et al. (2018) studies have indicated that the antibacterial activity of ZnO nanoparticles against *Staphylococcus aureus* and *Escherichia coli* increased with the decrease in their size from 250 to 80, 40, and 20 nm due to an increased reactive oxygen species generation and membrane damage in bacteria [11,12]. Different synthesis methods as sol–gel, hydrothermal, simple thermal sublimation, vapor–liquid–solid, double-jet precipitation, self-combustion, and "green synthesis" have been used to obtain ZnO nanorods, nanospheres, nanotubes, nanowires, and nanoneedles [13–15]. The control of synthesis conditions and parameters is very important in order to obtain homogeneous NPs, since antimicrobial activity is highly influenced by NPs' morphology, structure, and shape. Thus, in this work, a new controlled methodology to synthesize homogenous antimicrobial hollow ZnO nanotubes was developed based on the combination of electrospinning and atomic layer deposition technologies. Electrospinning (EP) is an efficient, simple, cost-effective, and scalable technique to generate polymeric fibers. The obtaining of the fibers occurs when a voltage is applied to the polymer solution, obtaining a flow with a conical structure known as the "Taylor Cone", where the solvent evaporates during the process to finally obtain thin structures with a high specific area [16,17]. On the other hand, the atomic layer deposition (ALD) is a technique that allows the fabrication of nanometric layers of a great variety of materials in different substrates [18]. This technique consists in the generation of thin films by introducing sequentially and cyclically two or more precursors in gas phase, under conditions of controlled temperature and pressure, where the precursors react chemically with the surface of a substrate, allowing the formation of atomic-scale monolayers [18,19]. Generally, a metal–organic precursor and a co-reactant as an oxygen source or as reducing agent are used [20]. One of the advantages that most attracts the attention of this technique is the ability to generate a unique uniform deposition, which allows the thickness of the film to be controlled by the amount of ALD cycles and, in addition, complex three-dimensional surfaces can be uniformly coated. These characteristics give it a great versatility that have allowed its application in a wide variety of areas, such as microelectronics, energy storage systems, water treatment, catalysis, and medicine and biology [21–29]. Nevertheless, the combination of EP and ALD has been scarcely used to synthesize nanoparticles with antimicrobial purposes. Furthermore, an antimicrobial bilayer structure was developed by applying a polymeric coating containing synthesized ZnO nanotubes over a polymeric substrate.

2. Materials and Methods

2.1. Polymers, Chemicals, and Microorganisms

Diethylzinc ($Zn(C_2H_5)_2$, DEZn, min. 95%), in a 50 mL Swagelok® cylinder was purchased from Strem Chemicals Inc. (Newburyport, MA, USA). Gohsenol AH-17 polyvinyl alcohol (PV) (saponification degree 97–98.5% and viscosity 25–30 mPa.s) was obtained from The Nippon Synthetic Chemical Co. (Osaka, Japan). Zinc oxide nanoparticles (ZnONP) were purchased from Sigma-Aldrich. Commercial acryl-based coating Elvacite 2010 was purchased from Lucite International (Chile).

Gram-negative *Escherichia coli* ATCC 25,922 and Gram-positive and *Staphylococcus aureus* ATCC 25,923 bacteria were chosen as bacteria strain models. Bacterial strains were obtained from Biotechnology and Applied Microbiology Laboratory (LAMAP) (Santiago, Chile) and stored in

glycerol 30% at −80 °C until needed. For experimental use, the stock cultures were maintained in tryptone soy agar slants at 4 °C and transferred monthly. Prior to each experiment, a loopful of each strain was transferred to 5 mL of tryptone soy agar and incubated at 37 °C for 16 h to obtain fresh early-stationary phase cells.

The cytopathogenic F9 strain of Feline calicivirus (FCV, ATCC VR-782) was propagated and assayed on CRFK (Crandell Reese Feline Kidney) cells from ATCC (CCL-94). Semi-purified stocks were subsequently produced on CRFK cells by the centrifugation of infected cell lysates at 660× g for 30 min after 2–3 days post-infection. Infectious viruses were calculated by determining the 50% tissue culture infectious dose (TCID50) using the Spearmen–Karber method [30].

2.2. Development of ZnO Hollow Nanotubes (ZnO_{NT})

Electrospun poly(vinyl alcohol) nanofibers (PV$_f$) were developed by using an electrospinning system (Spraybase®power Supply Unit, Maynooth, Ireland), according to our previous work [31]. Poly(vinyl alcohol) solution at 8% (*w/v*) was prepared in distilled water with stirring at 90 °C. The polymeric solution was transferred in a 5 mL plastic syringe and connected through a polytetrafluoroethylene tube to a stainless steel needle of 1.6 mm diameter charged by a high-voltage power supply with a range of 0–20 kV. Finally, PV$_f$ nanofibers were obtained using 1.5 mL/h as the flow rate and 10 cm as the distance between the tip needle and the collector.

Subsequently, PV$_f$ nanofibers behaved as a template for the preparation of hollow ZnO$_{NT}$. Zinc oxide was deposited over PV$_f$ fibers using a Savannah S100 ALD reactor (Ultratech, San Jose, CA, USA) maintained at 150 °C. Water (H_2O) and diethylzinc ($Zn(C_2H_5)_2$, DEZn) were used as precursors. The atomic layer deposition (ALD) pulse lengths were set at 0.12 s for DEZn dosing, 3 s for N_2 purging, 0.15 s for H_2O dosing, and 3 s for N_2 purging [32]. Deposition based on 300 and 500 cycles was performed in order to investigate the effect of the number of ALD cycles on the thickness and quality of the coating.

Lastly, two methodologies were tested to remove the polymer from the inner zone of the metal oxide-deposited nanofibers. (i) Process A: ZnO-PV$_f$ suffered a thermal treatment process in order to remove PV polymer from the inner side. Deposited nanofibers were calcinated at 450 °C and 600 °C during 1 h at air atmosphere. (ii) Process B: Thanks to the hydrosoluble nature of PV polymer, an alternative polymeric removal process was attempted by washing ZnO-deposited nanostructures with hot distilled water. Samples were sonicated into distilled water at 90 °C for 1 h. The sample that resulted from the washing process was named (ZnO-PV$_f$)-B.

2.3. Characterization of ZnO Hollow Nanotubes

During the three stages for obtaining hollow ZnO$_{NT}$, each structure was observed using scanning electron microscopy, SEM (Zeiss EVO MA10 SEM, Oberkochen, Germany), at 20 kV. Developed ZnO$_{NT}$ were also analyzed through transmission electron microscopy, TEM (Hitachi HT7700 high resolution TEM, Chiyoda, Tokyo, Japan), at 100 kV.

X-ray Diffraction (XRD) patterns were measured using a Siemens diffractometer D5000 (Siemens AG, Erlangen, Germany) (30 mA and 40 kV) using Cu Ka (λ = 1.54 Å) radiation at room temperature. All scans were performed in a 2θ range of 2–80° at 0.02° s^{-1}.

The small-angle X-ray scattering (SAXS) measurement was performed using a Bruker N8 Horizon model equipped with a Cu source (radiation Kα_1, λ = 1.54060 Å, radiation Kα_2, λ = 1.54439 Å) and 2D VÅNTEC-500 detector and MONTEL optics (Bruker AXS GmbH, Karlsruhe, Germany). The data were acquired in the q-range from 0.012 to 0.37 Å^{-1} with a measurement time of 7200 s in vacuum (2 mbar) and at room temperature. The generator was operated at 1 kW (40 kV and 25 mA). The data processing and analysis were performed using a Bruker DIFFRAC.SAXS program (Bruker AXS GmbH, Karlsruhe, Germany) that can fit and evaluate the size of the structures assuming different geometries.

Thermogravimetric analyses (TGA) were carried out through a Mettler Toledo Gas Controller GC20 Stare System TGA/DCS (Schwerzenbach, Switzerland). First, 5–6 mg of each sample was heated from 30 to 600 °C at 10 °C/min under nitrogen atmosphere with a flow rate of 50 mL min^{-1}.

2.4. Development of Antimicrobial Bilayer Systems Containing ZnO Nanoparticles

Two antimicrobial bilayer structures were obtained by coating acrylic solutions containing zinc oxide nanotubes (ZnO_{NT}) at 0.5 and 1 wt % with respect to acrylic polymer over an extruded 32 μm-polyethylene (PE) substrate film. According to the ZnO_{NT} concentrations, the bilayer structures were named 0.5ZnO_{NT}-Acry/PE and 1ZnO_{NT}-Acry/PE. ZnO_{NT} were dispersed in the 20 wt % acrylic solution under ethyl acetate. Before the coating process, a corona treatment on PE films was carried out by using a FT-350 mm Model equipment (HT, Taiwan) to improve coating adherence. Coatings were performed with a RK-Print multicoater equipment model K303 (RK Print Coat Instruments Ltd., Litlington, UK) by applying 6 mL of each solution onto PE films using a stainless steel rod No. 4 at 5 m min^{-1}. Finally, coatings were dried during one minute at room temperature, and their thickness values were approximately 3–4 μm. In order to compare the antimicrobial effectiveness of ZnO_{NT}-containing films, bilayer structures with commercial zinc oxide nanoparticles (ZnONP) were also analyzed (the TEM micrograph of ZnONP can be found in Figure S3 in Supplementary Material). These bilayer structures were obtained following the same method described above, and films were named 0.5ZnONP-Acry/PE and 1ZnONP-Acry/PE, when containing 0.5 and 1 wt % of ZnONPs, respectively.

2.5. Scanning Electronic Microscopy (SEM) Characterization of Bilayer Structure

SEM micrographs of the bilayer structure containing the highest concentration of ZnO_{NT} were performed through a SEM (Zeiss EVO MA10 SEM) scanning microscope with an accelerating voltage at 10 kV. Bilayer films were firstly cryofractured by previous immersion into liquid nitrogen. Subsequently, films were coated with gold palladium with a Anatech Hummer 6.2 sputtering system (Anatech USA, Sparks, USA). SEM micrographs of the cross-sections of the films were taken.

2.6. Antibacterial Activity of Bilayer Nanocomposites

The antibacterial activities of ZnO_{NT}-Acry/PE and ZnONP-Acry/PE bilayer films were tested against Gram-negative bacteria *Escherichia coli* and Gram-positive bacteria *Staphylococcus aureus* according the Japanese Industrial Standard JIS Z 2801:2000 [33]. Test inoculums of each microorganism with a final concentration of 10^5 CFU mL^{-1} were prepared. Film samples were prepared cutting coated and uncoated PE films in squares of 5 cm × 5 cm, while cover films were prepared cutting uncoated PE films in squares of 4 cm × 4 cm. Three specimens of each test sample and cover films were prepared and sterilized with 70% ethanolic solution. Test samples were collocated in a sterile Petri dish maintaining the coated surface exposed outside, and 400 μL of test inoculums were pipetted over them. Cover films were collocated upon test samples, avoiding the leak of test inoculums by edges, and the Petri dishes covered with the lid were incubated at 35 °C and of 93.2% relative humidity (RH) for 24 h. The test inoculum of test samples was recovered by manually stirring 10 mL of sterile phosphate buffer added in each Petri dish, and 10-fold dilutions with PBS were done. Then, 1 mL of each dilutions was placed in sterile Petri dishes and 20 mL of tryptic soy agar was poured in order to count the viable cells after incubating the Petri dishes at 35 °C for 48 h.

### 2.7. Determination of Virucidal Activity

Determination of the virucidal activities of films containing 0.5 and 1% wt. % of ZnO nanostructures were performed by adapting the standard. Briefly, 50 μL of FCV suspension diluted in PBS (phosphate buffer solution) at 3 and 6 log TCID$_{50}$/mL was placed onto the test films (3 cm × 3 cm) and covered by a piece of low-density polyethylene (LDPE) (2.5 cm × 2.5 cm). Samples were stored overnight at 25 °C at 100% RH. Thereafter, the top film was lifted, and the virus droplet-exposed sides were recovered and 10-fold diluted with PBS. Then, infectious viruses were enumerated by cell culture assay as described above. Each treatment was done in triplicate. The virus decay titer was calculated as $\log_{10} (N_x/N_0)$,

where N_0 is the infectious virus titer for untreated films and N_x is the infectious virus titer for treated films [30].

3. Results and Discussion

### 3.1. Morphological Characterization of ZnO_{NT} and Nanocomposites Containing ZnO_{NT}

The morphologies of ZnO nanostructures obtained following different conditions during ALD and polymer removal processes were studied using TEM and SEM microscopies. Successful zinc oxide hollow nanotubes, from now on called ZnO_{NT}, were developed by the calcination process at 450 °C of deposited fibers during 500 cycles of deposition. The resulting images revealed that the number of ALD cycles (300 and 500) and the temperature of calcination (Process A: 450 °C and 600 °C) were the main parameters to optimize the development of homogeneous hollow ZnO nanotubes. Figure 1 shows TEM images of resulting nanostructures by applying these conditions. The resulting morphologies distinguished that the calcination temperature was a critical parameter that determined the formation of the nanotubular structure. When the calcination temperature occurred at 600 °C, the system failed to retain the shape of a nanotube for both numbers of cycles, forming chains of ZnO nanoparticles (see Figure 1a,b). This necklace-like morphology has been previously observed for structures subjected to high calcination temperatures [32,34]. The increase in calcination temperature produced an increase in the size of the ZnO grains from 45 nm for 450 °C to approximately 200 nm for 600 °C. This abrupt change in grain size was primarily responsible for the collapse of tubular morphology. On the other hand, the application of a higher calcination temperature produced a more aggressive thermal decomposition of the polymer, causing fractures of the nanotubes due to the release of compounds (water and acetaldehyde by-products) [31].
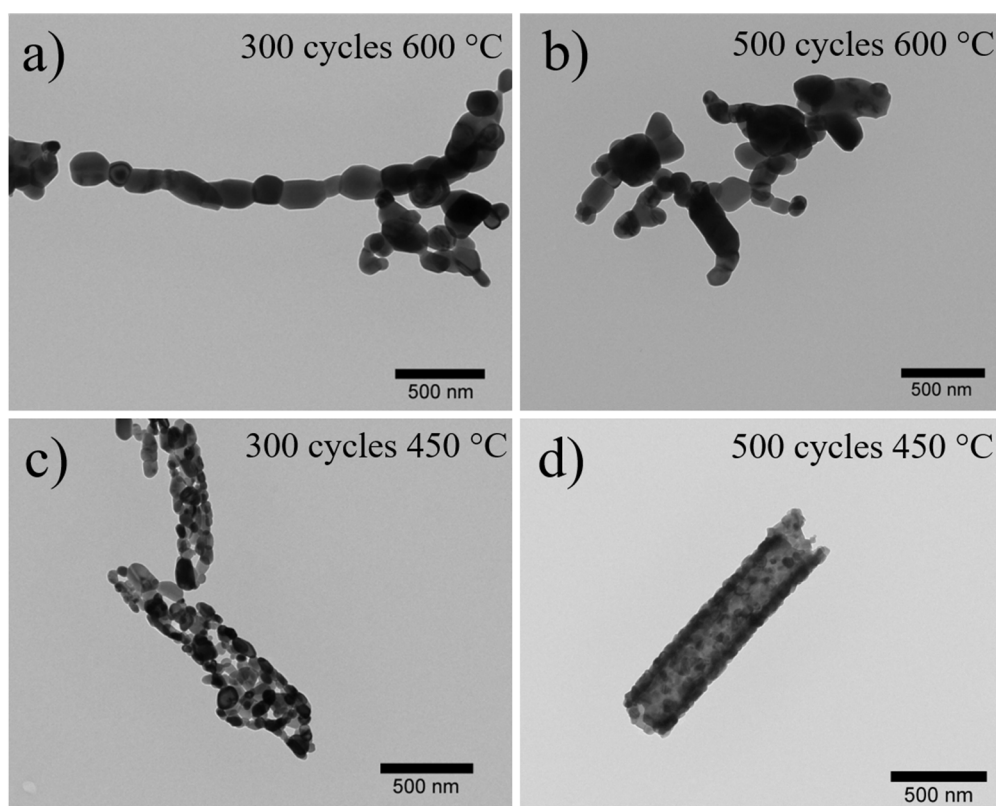
Figure 1. TEM images of ZnO nanostructures obtained by applying different conditions of number of cycles and temperature of calcination: (**a**) 300 cycles and 600 °C; (**b**) 500 cycles and 600 °C; (**c**) 300 cycles; and (**d**) 500 cycles and 450 °C.

Therefore, both the increase in grain size and the thermal decomposition of the polymer contributed to the shape of the nanotubes collapse at 600 °C. On the other hand, when the calcination occurred at 450 °C, the tubular morphology was maintained (Figure 1c,d).

It is interesting to highlight that although the samples obtained through 300 and 500 ALD cycles exhibited a tubular shape, when they were thermal treated at 450 °C, the sample with 500 ALD cycles presented the formation of a wall with a highly uniform coating (Figure 1d). Based on the aforementioned results, the optimal values for ZnO_{NT} synthesis were fixed at 500 ALD cycles and 450 °C as the number of cycles and the temperature for polymer removal, respectively. Figure 2a,b confirmed that the resulting nanotubes at these conditions exhibited an average wall thickness of 59.5 ± 7.9 nm with an internal diameter of approximately 178.2 nm. The corresponding histogram of wall thickness is presented in Figure 2c.
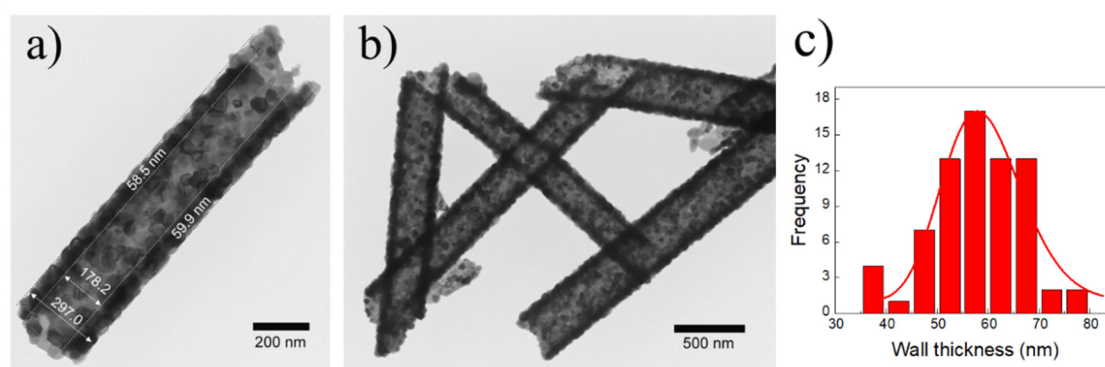
Figure 2. TEM images of ZnO_{NT} (500 ALD cycles and 450 °C as calcination temperature) at different magnifications: (**a**) 10 kx and (**b**) 20 kx; and (**c**) ZnO_{NT} wall thickness histogram.

ZnO_{NT} were also analyzed through SEM microscopy, and, as Figure 3a,b show, ZnO_{NT} presented a highly homogeneous morphology and hollow nature (additional SEM images are presented in Figure S1 in the Supplementary Material).
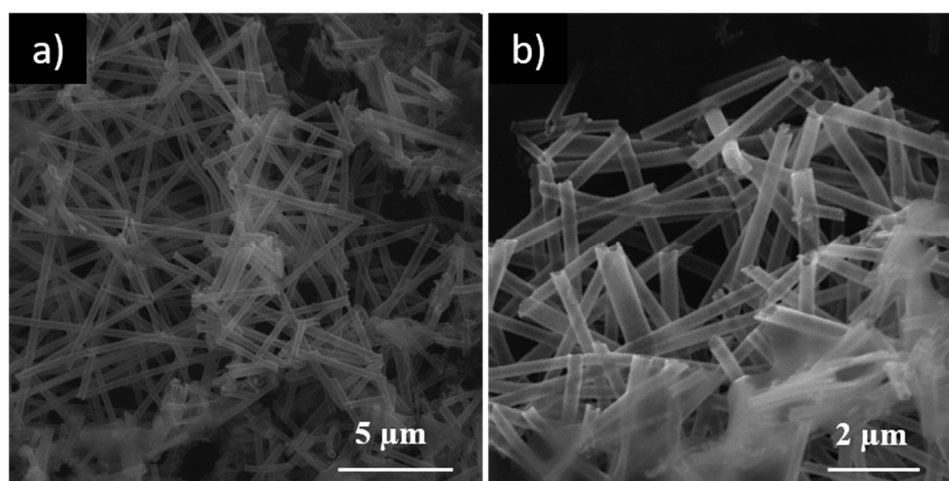

Figure 3. SEM micrographs of ZnO_{NT} at magnifications: (**a**) 10 kx; and (**b**) 20 kx.

The alternative polymer removal process through washing with distilled water at 90 °C (Process B) did not present satisfactory results. The stirring of deposited fibers under hot distilled water allowed a partial dissolution of the inner polymer, and the resulting polymer rate removal was very low, as the TGA results confirmed (next Section 3.3). Nevertheless, interesting TEM images of the sample that resulted from this washing process, (ZnO-PV_f)-B, are shown in Figure S2 in the Supplementary Material.

3.2. Structural Analysis of Nanostructures

Figure 4 shows the diffractograms of the structures during the obtaining process of the hollow ZnO_{NT}. Although the electrospinning process reduces polymer crystallinity, electrospun PV_f demonstrated a semi-crystalline nature through the presence of a sharp peak at $2\theta = 22.5°$, which is characteristic of a monoclinic PV crystal structure [35]. The deposition of this metal oxide over PV nanofibers (sample $ZnO-PV_f$) enhanced this polymer crystallinity, and a new characteristic PV crystalline peak was evidenced at 19.5° [31,35,36]. Probably, the electrospun PV fibers exposition to the ALD chamber temperature (150 °C) and further cooling allowed the reorganization of PV polymeric chains. Furthermore, new peaks related to zinc oxide appeared at $2\theta = 31.8$, 34.4, 36.2, 56.7 and 62.9, confirming the deposition of this metal oxide by ALD. After the calcination process, these peaks have definitely increased their intensities, and other ZnO characteristic peaks were present at $2\theta = 47.6$, 66.3, 67.8, 69.1, 72.4, and 76.9°. This diffractogram has clearly shown evidence that hollow ZnO_{NT} presented the hexagonal wurtzite crystal structure [34,37] as commercial ZnO nanoparticles. The principal peaks of both ZnO nanostructures correspond to a quite pure hexagonal stage wurtzite (Joint Committee on Powder Diffraction Standards JCPDS card No. 89-1397). The thermal treatment of calcination not only allowed the total PV polymer removal but also this resulting crystal structure. Sharp and narrow diffractive peaks indicated the efficient crystallization process.

Small-angle X-ray scattering (SAXS) allows the measurement of the scattering behavior at smaller angles. This analysis results assumed a core–shell cylinder with a thickness of 61.31 nm and a radius of 181.72 nm, confirming the measurements obtained through TEM and SEM images.
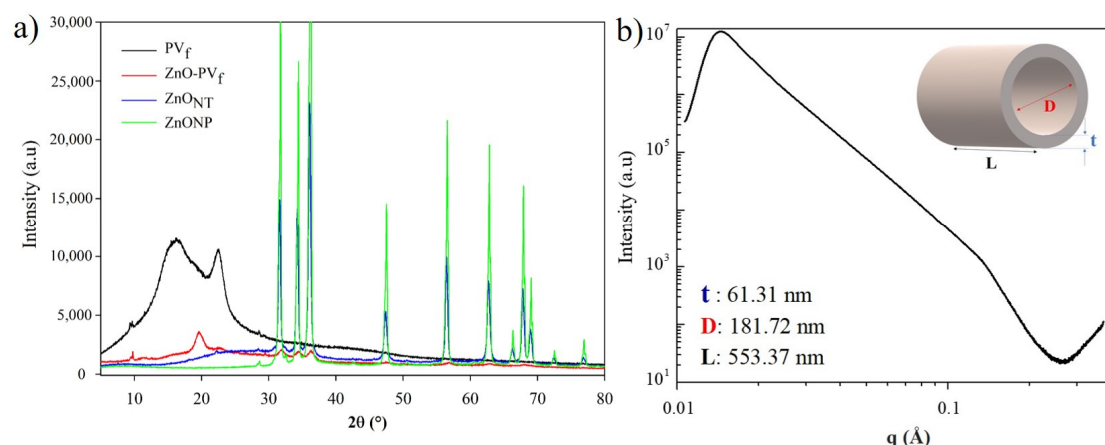
Figure 4. (**a**) XRD diffraction patterns of electrospun polyvinyl alcohol (PV) fibers (PV_f), coated nanofibers ($ZnO-PV_f$), hollow zinc oxide nanotubes (ZnO_{NT}), and commercial zinc oxide nanoparticles (ZnONP); (**b**) I(q)-q plot of ZnO_{NT} structure obtained by small-angle X-ray scattering (SAXS).

3.3. Thermogravimetric Analyses of Nanostructures

Each process for obtaining hollow ZnO_{NT} was analyzed through thermogravimetric analysis, and the TGA curves are shown in Figure 5. The mass loss with respect to temperature of PV_f, deposited $ZnO-PV_f$, and $(ZnO-PV_f)$-B provided evidence of the characteristic degradation process of PV polymer in three stages: (i) the dehydration of samples below 100 °C; (ii) the separation of side groups of PV polymer and the loss of hydrogen in chains of the polymer and oxygen bond in C-O groups between 220 and 390 °C; and (iii) the degradation of the principal polymeric chain between 390 and 480 °C [38,39]. After the dehydration process, deposited nanofibers $ZnO-PV_f$ and $(ZnO-PV_f)$-B presented a decomposition temperature onset lower than PV_f nanofibers at approximately 180 and 220 °C, respectively. This fact was probably due to the catalytic nature of ZnO that anticipated PV decomposition [40].
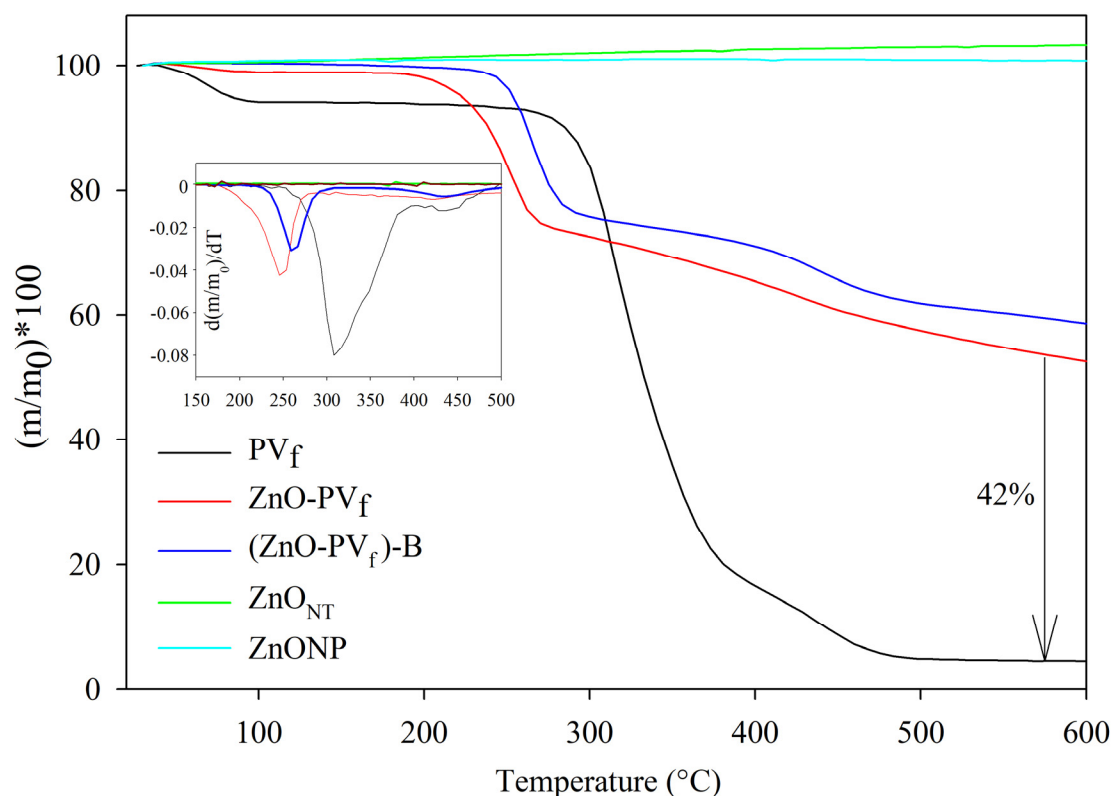
Figure 5. Weight loss with temperature of developed nanostructures (insert: derivative of weight loss with respect to temperature).

TGA analysis of ZnO-PV$_f$ also revealed the ALD-deposited process on PV nanofibers resulted in ZnO of 41.2 wt. % approximately, and the PV removal process through washing [sample (ZnO-PV$_f$)-B] was not effective because only 12.3 wt. % of polymer was removed. A previous work based on the development of TiO$_2$ nanotubes at the same ALD process conditions presented similar results, which provided evidence of the efficiency and reproducibility of method independently of the type of metal oxide precursors used [31]. TGA analysis was also used to confirm the total elimination of the PV polymer after the calcination and obtaining the hollow ZnO$_{NT}$ nanotubes. This result was evidenced because ZnO$_{NT}$ presented the same TGA curve as commercial ZnONP, demonstrating that ZnO$_{NT}$ nanostructures were PV polymer-free.

3.4. Morphological Analysis of Bilayer Nanocomposites Containing ZnO$_{NT}$

Figure 6 shows SEM micrographs of the cross-section of the bilayer structure 1ZnO$_{NT}$-Acry/PE at different magnifications. Both layers with their corresponding thickness can be clearly evidenced in Figure 6a, and the effectiveness of the coating process in order to obtain a homogeneous second layer was confirmed. The images indicated that the antimicrobial coating containing ZnO$_{NT}$ presented a smooth surface and a thickness of approximately 3–4 μm. The application of this acrylic polymeric coating containing ZnO$_{NT}$ over the PE substrate allowed the development of an antimicrobial material by incorporating activity in the contact layer. This bilayer system reduces the necessary amount of the antimicrobial ZnO$_{NT}$ to provide the functional activity [41].

The presence of the hollow ZnO$_{NT}$ was not greatly observed due to the low concentration of these nanostructures. Nevertheless, Figure 6e shows a particle that could be a nanotube due to its dimensions, and Figure 6f seems to present a hole derived from the absence of a nanotube after film fracture.
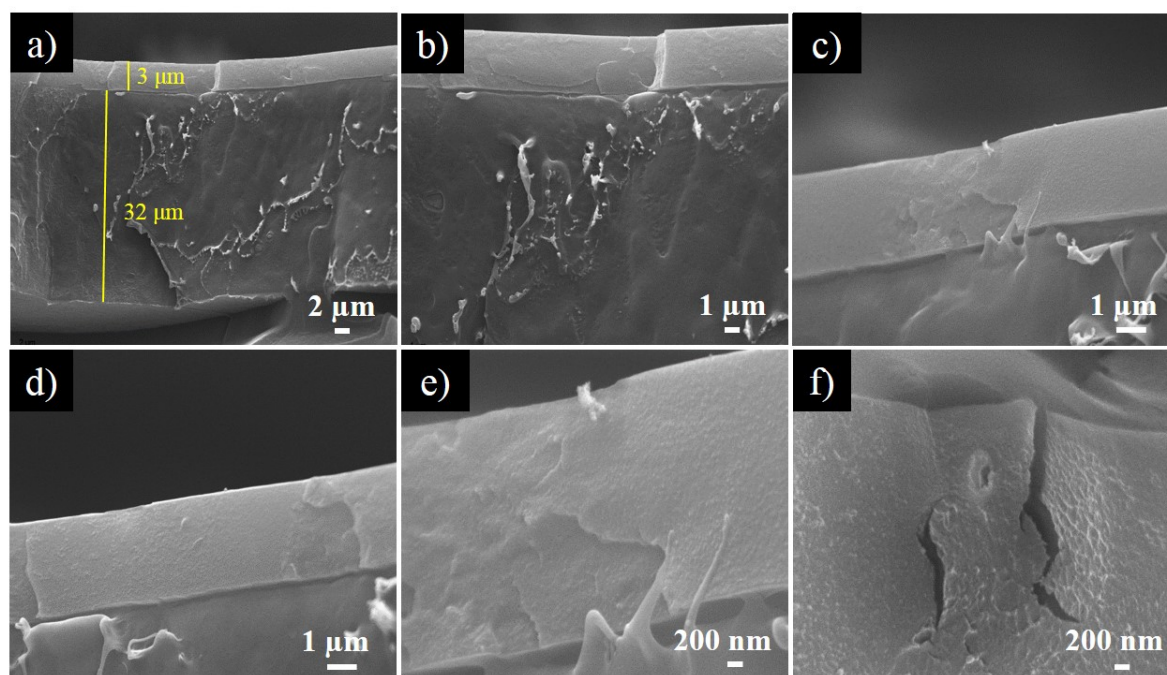
Figure 6. SEM micrographs of bilayer composite $1ZnO_{NT}$-Acry/PE at different magnifications: (**a**) 5 kx; (**b**) 10 kx; (**c,d**) 20 kx; (**e,f**) 50 kx.

3.5. Antibacterial Activity Results

Table 1 shows antibacterial results of active bilayer films expressed in log reduction of cells/cm^2. Bilayer structures of Acry/PE containing ZnO_{NT} or ZnONP have shown antibacterial activities against the evaluated microorganisms. Antimicrobial activity increased as the concentration of nanostructures increased, and ZnO_{NT}-Acry/PE materials presented better antimicrobial activity against both bacteria compared with ZnONP-Acry/PE films. According to JIZ Z 2801:2000, an antimicrobial activity of R > 2.0 log cells/cm^2 is required to demonstrate the antimicrobial efficacy of active materials [42]. Except for the coating 1ZnONP-Acry against *S. aureus*, both antimicrobial coatings with 1 wt % of ZnO_{NT} or ZnONPs presented a log reduction > 2.0, demonstrating the great antimicrobial activity of this metal oxide. Specifically, the bilayer structure $1ZnO_{NT}$-Acry/PE resulted in the total inhibition of *E. coli*. Several mechanisms have described ZnO antimicrobial activity, including cell damage through their interaction with the microorganisms, ions release from zinc oxide, and the reactive oxygen species (ROS) formation by the activation of this metal oxide [43,44]. In this case, the possible mechanism could be the interaction of ZnO_{NT} and ZnONP with the bacteria due to the conditions of antimicrobial assay. The antimicrobial activity efficacy of zinc oxide nanoparticles is influenced by morphology, size, and surface energy. The morphology of ZnO nanoparticles is greatly determined by synthesis conditions such as solvents, temperature, pH, and precursor types, which are employed in precipitation, sol–gel, and solvothermal techniques in order to obtain circular, tubular, or irregular morphologies [13,45]. In this study, ZnO_{NT} morphology, which had a high aspect ratio due to their hollow structure and wall thickness, was controlled by electrospinning and ALD parameters. The high aspect ratio of ZnO_{NT} allowed exhibiting a strong antibacterial activity against Gram-positive and negative bacteria compared to ZnONP. A similar result was obtained with hollow titanium dioxide nanotubes against *Escherichia coli*. In this study, a concentration of TiO_2 nanotubes lower than TiO_2 nanoparticles was required to obtain a total reduction of Gram-negative bacteria.

Table 1. Antibacterial results of coated PE containing ZnO_{NT} and ZnONP at 0.5 and 1 wt. % against different microorganisms.

Microorganism	*Escherichia coli*		*Staphylococcus aureus*	
Sample	Cell Conc. cells/cm^2	Log Reduction	Cell Conc. cells/cm^2	Log Reduction
PE	4.69×10^4	-	5.28×10^5	-
0.5ZnO$_{NT}$-Acry/PE	2.22×10^2	2.32	2.35×10^4	1.35
1ZnO$_{NT}$-Acry/PE	0.00	4.67	1.85×10^3	2.46
0.5ZnONP-Acry/PE	1.08×10^4	0.64	1.07×10^5	0.69
1ZnONP-Acry/PE	3.13×10^1	3.18	2.80×10^4	1.27

In the case of materials with ZnONP-containing coating, the antimicrobial activity was similar against both bacteria, and the structure 1ZnONP-Acry/PE showed evidence of the highest activity against *E. coli*, with a log reduction of 2.32 cells/cm^2. Both films presented higher effectiveness against Gram-negative bacteria.

On the other hand, the highest antimicrobial activity against *S. aureus* was obtained with 1ZnO$_{NT}$-Acry/PE film with a log reduction of 2.46 cells/cm^2. The lower antimicrobial activity of nanostructures against *S. aureus* is due to its intracellular antioxidant content as well as the presence of potent detoxification agents [10]. Additionally, the difference of the cell wall structure to both bacteria plays an important role in the antimicrobial activity of nanoparticles, which had been observed with other metal oxides [46]. Gram-negative bacteria have a thin peptidoglycan layer that facilitate the mobility of metal ion nanoparticles to the cell and assist the interaction between ZnO nanoparticles with bacterial cell walls, while Gram-positive bacteria have a thick layer of peptidoglycan that protect and cause more resistance. In addition, the negative charge of the lipopolysaccharide layer in Gram-negative bacteria leads to intracellular damages and the destruction of proteins and DNA [47].

Generally, the results showed a high antibacterial activity in films coated with ZnO$_{NT}$. The concentration, size, and shape of hollow ZnO nanotubes directly influenced the antimicrobial efficacy of zinc oxide, where a larger surface area and higher concentration of ZnO nanotubes in the PE-NT were responsible for the highest antibacterial activity [13].

3.6. Antiviral Activity against Norovirus Surrogate

In the current study, FCV, a norovirus surrogate broadly used for testing disinfectants (EPA (Environmental Protection Agency), 2002) and virucidal films [48–50], was exposed to ZnO-containing films for 24 h following the ISO 22196:2011. As Table 2 shows, unfortunately, none of these evaluated nanocomposites showed antiviral activity under the experimental conditions tested. FCV concentrations control and in contact with nanocomposites did not present significant differences. Currently, some metallic nanoparticles as silver and copper with demonstrated virucidal activity have been used to develop antiviral polymers. Specifically, Martínez et al. (2013) have applied silver-infused polylactide (PLA) films for the inactivation of FCV [49]. The antiviral activity of silver-PLA films was dose-dependent, where increasing concentrations of silver showed an increased reduction in viral titers. Nevertheless, as observed in this study, FCV was less susceptible than *Salmonella*, suggesting a higher resistance of viruses to antimicrobial compounds than bacteria. In line, micrometer-sized magnetic hybrid colloid activated with AgNPs reduced the infectivity of murine norovirus, which is another norovirus surrogate, by more than 2 log, while more than a 6 log reduction was reported for *E. coli* [50,51]. Similarly, AgNP-containing fiber mats reduced MNV (novel mouse norovirus) infectivity by only 0.86 log while under the same conditions, and no viable counts of *Salmonella enterica* and *Listeria monocytogenes* were recorded [52].

Table 2. Antiviral effect of ZnO films on feline calicivirus (FCV) titers (log $TCID_{50}$/mL) after overnight incubation at 25 °C at 100% relative humidity (RH) following ISO 22196:2011. PE: polyethylene, $TCID_{50}$: tissue culture infectious dose

	High FCV Concentration		Low FCV Concentration	
Sample	**Log $TCID_{50}$/mL**	**Reduction**	**Log $TCID_{50}$/mL**	**Reduction**
PE	6.66 ± 0.29		3.91 ± 0.38	
$0.5ZnO_{NT}$-Acry/PE	6.57 ± 0.22	0.08	3.78 ± 0.19	0.13
$1ZnO_{NT}$-Acry/PE	6.70 ± 0.25	-0.04	4.03 ± 0.19	-0.13
0.5ZnONP-Acry/PE	6.57 ± 0.25	0.08	3.53 ± 0.07	0.38
1ZnONP-Acry/PE	6.24 ± 0.38	0.42	3.53 ± 0.14	0.38

4. Conclusions

Hollow zinc oxide nanotubes with an average diameter of 180 nm and thickness of approximately 60 nm were successfully obtained through the combination of electrospinning and atomic layer deposition processes. A total of 500 ALD cycles of diethyl zinc and water as precursors over electrospun polyvinyl alcohol fibers followed by a calcination process at 450 °C resulted in homogenous hollow zinc oxide nanotubes. Subsequently, bilayer systems composed by an acrylic polymeric coating containing as-synthesized zinc oxide nanotubes over a polyethylene substrate were successfully developed. Antimicrobial analysis revealed that the antimicrobial effectiveness was dependent on zinc oxide concentration and the antimicrobial materials presented the highest activity against Gram-negative bacteria. When compared to a bilayer system containing commercial zinc oxide nanoparticles, materials with zinc oxide nanotubes presented higher antimicrobial effectiveness probably because their tubular morphology presented a higher specific surface area and lower aggregation than commercial spherical zinc oxide nanoparticles.

Supplementary Materials: The following are available online at http://www.mdpi.com/2079-4991/10/3/503/s1, Figure S1. SEM micrographs (3D-SEM) of hollow ZnO_{NT} at magnifications: (**a**) 15 kx; and (**b**) 10 kx; Figure S2. TEM images of ZnO-PV_f after washing process: (ZnO-PV_f)-B; and Figure S3. TEM image of commercial ZnONP.

Author Contributions: C.L.d.D. and J.E. proposed and supervised the research. C.P.V. and P.M. worked on the electrospinning, atomic layer deposition, and calcination processes to obtain hollow zinc oxide nanotubes. Characterization measurements including antimicrobial activity analysis were carried out by previous four authors. I.F. and G.S. performed antiviral analysis. All authors collaborated with the writing. All authors have read and agreed to the published version of the manuscript.

Conflicts of Interest: The authors declare no conflict of interest.

References

1. Colavecchio, A.; Cadieux, B.; Lo, A.; Goodridge, L.D. Bacteriophages contribute to the spread of antibiotic resistance genes among foodborne pathogens of the Enterobacteriaceae family—A review. *Front. Microbiol.* **2017**, *8*, 1108. [CrossRef]
2. Mahira, S.; Jain, A.; Khan, W.; Domb, A.J. Chapter 1. Antimicrobial Materials—An Overview. In *Antimicrobial Materials for Biomedical Applications*; Royal Society of Chemistry: London, UK, 2019; pp. 1–37.
3. Jiménez, A.; Vargas, M.; Chiralt, A. Antimicrobial Nanocomposites for Food Packaging Applications: Novel Approaches. In *Novel Approaches of Nanotechnology in Food*; Elsevier: Amsterdam, The Netherlands, 2016; pp. 347–386.
4. Fasihnia, S.H.; Peighambardoust, S.H.; Peighambardoust, S.J. Nanocomposite films containing organoclay nanoparticles as an antimicrobial (active) packaging for potential food application. *J. Food Process. Preserv.* **2018**, *42*, e13488. [CrossRef]

5. Ebrahimi, Y.; Peighambardoust, S.J.; Peighambardoust, S.H.; Karkaj, S.Z. Development of antibacterial carboxymethyl cellulose-based nanobiocomposite films containing various metallic nanoparticles for food packaging applications. *J. Food Sci.* **2019**, *84*, 2537–2548. [CrossRef] [PubMed]

6. Gold, K.; Slay, B.; Knackstedt, M.; Gaharwar, A.K. Antimicrobial activity of metal and metal-oxide based nanoparticles. *Adv. Ther.* **2018**, *1*, 1700033. [CrossRef]

7. Dumbrava, A.; Berger, D.; Matei, C.; Prodan, G.; Aonofriesei, F.; Radu, M.D.; Moscalu, F. New Composite nanomaterials with antimicrobial and photocatalytic properties based on silver and zinc oxide. *J. Inorg. Organomet. Polym. Mater.* **2019**, *29*, 2072–2082. [CrossRef]

8. Tan, L.-Y.; Sin, L.T.; Bee, S.-T.; Ratnam, C.T.; Woo, K.-K.; Tee, T.-T.; Rahmat, A.R. A review of antimicrobial fabric containing nanostructures metal-based compound. *J. Vinyl Addit. Technol.* **2019**, *25*, E3–E27. [CrossRef]

9. Vimbela, G.; Ngo, S.M.; Fraze, C.; Yang, L.; Stout, D.A. Antibacterial properties and toxicity from metallic nanomaterials. *Int. J. Nanomed.* **2017**, *12*, 3941–3965. [CrossRef]

10. Espitia, P.J.P.; de Soares, N.F.F.; dos Coimbra, J.S.R.; de Andrade, N.J.; Cruz, R.S.; Medeiros, E.A.A. Zinc oxide nanoparticles: Synthesis, antimicrobial activity and food packaging applications. *Food Bioprocess Technol.* **2012**, *5*, 1447–1464. [CrossRef]

11. Appierot, G.; Lipovsky, A.; Dror, R.; Perkas, N.; Nitzan, Y.; Lubart, R.; Gedanken, A. Enhanced antibacterial activity of nanocrystalline ZnO due to increased ROS-mediated cell injury. *Adv. Funct. Mater.* **2009**, *19*, 842–852. [CrossRef]

12. Verma, S.K.; Jha, E.; Panda, P.K.; Das, J.K.; Thirumurugan, A.; Suar, M.; Parashar, S.K.S. Molecular aspects of core-shell intrinsic defect induced enhanced antibacterial activity of ZnO nanocrystals. *Nanomedicine* **2018**, *13*, 43–68. [CrossRef]

13. Sirelkhatim, A.; Mahmud, S.; Seeni, A.; Kaus, N.H.M.; Ann, L.C.; Bakhori, S.K.M.; Hasan, H.; Mohamad, D. Review on zinc oxide nanoparticles: Antibacterial activity and toxicity mechanism. *Nano Micro Lett.* **2015**, *7*, 219–242. [CrossRef] [PubMed]

14. Agarwal, H.; Venkat Kumar, S.; Rajeshkumar, S. A review on green synthesis of zinc oxide nanoparticles—An eco-friendly approach. *Resour. Technol.* **2017**, *3*, 406–413. [CrossRef]

15. Shah, M.; Fawcett, D.; Sharma, S.; Tripathy, S.K.; Poinern, G.E.J. Green synthesis of metallic nanoparticles via biological entities. *Materials* **2015**, *8*, 7278–7308. [CrossRef] [PubMed]

16. Bhardwaj, N.; Kundu, S.C. Electrospinning: A fascinating fiber fabrication technique. *Biotechnol. Adv.* **2010**, *28*, 325–347. [CrossRef] [PubMed]

17. Kenry; Lim, C.T. Nanofiber technology: Current status and emerging developments. *Prog. Polym. Sci.* **2017**, *70*, 1–17. [CrossRef]

18. Johnson, R.W.; Hultqvist, A.; Bent, S.F. A brief review of atomic layer deposition: From fundamentals to applications. *Mater. Today* **2014**, *17*, 236–246. [CrossRef]

19. Oviroh, P.O.; Akbarzadeh, R.; Pan, D.Q.; Coetzee, R.A.M.; Jen, T.C. New development of atomic layer deposition: Processes, methods and applications. *Sci. Technol. Advan. Mater.* **2019**, *20*, 465–496. [CrossRef]

20. Parsons, G.N.; George, S.M.; Knez, M. Progress and future directions for atomic layer deposition and ALD-based chemistry. *Mrs Bulletin* **2011**, *36*, 865–871. [CrossRef]

21. Waduge, W.L.I.; Chen, Y.J.; Zuo, P.; Jayakodiarachchi, N.; Kuech, T.F.; Babcock, S.E.; Evans, P.G.; Winter, C.H. Solid-phase epitaxy of perovskite high dielectric PrAlO3 films grown by atomic layer deposition for use in two-Dimensional electronics and memory devices. *ACS Appl. Nano Mater.* **2019**, *2*, 7449–7458. [CrossRef]

22. Tiurin, O.; Ein-Eli, Y. A critical review: The impact of the battery electrode material substrate on the composition and properties of atomic layer deposition (ALD) coatings. *Adv. Mater. Interfaces* **2019**, *6*, 1901455. [CrossRef]

23. Feng, J.H.; Xiong, S.; Wang, Y. Atomic layer deposition of TiO2 on carbon-nanotube membranes for enhanced capacitive deionization. *Sep. Purif. Technol.* **2019**, *213*, 70–77. [CrossRef]

24. Song, Z.N.; Fathizadeh, M.; Huang, Y.; Chu, K.H.; Yoon, Y.M.; Wang, L.; Xu, W.W.L.; Yu, M. TiO2 nanofiltration membranes prepared by molecular layer deposition for water purification. *J. Membr. Sci.* **2016**, *510*, 72–78. [CrossRef]

25. Yang, H.M.; Chen, Y.; Qin, Y. Application of atomic layer deposition in fabricating high-efficiency electrocatalysts. *Chinese J. Catal.* **2020**, *41*, 227–241. [CrossRef]

26. Chen, Y.; Yuchi, Q.X.; Li, T.; Yang, G.H.; Miao, J.J.; Huang, C.Y.; Liu, J.Y.; Li, A.P.; Qin, Y.; Zhang, L.B. Precise engineering of ultra-thin Fe2O3 decorated Pt-based nanozymes via atomic layer deposition to switch off undesired activity for enhanced sensing performance. *Sens. Actuators B Chem.* **2020**, *305*. [CrossRef]

27. Hyde, G.K.; McCullen, S.D.; Jeon, S.; Stewart, S.M.; Jeon, H.; Loboa, E.G.; Parsons, G.N. Atomic layer deposition and biocompatibility of titanium nitride nano-coatings on cellulose fiber substrates. *Biomed. Mater.* **2009**, *4*. [CrossRef]

28. Yao, L.T.; Wu, X.H.; Wu, S.Y.; Pan, X.Y.; Tu, J.Y.; Chen, M.Y.; Al-Bishari, A.M.; Al-Baadani, M.A.; Yao, L.L.; Shen, X.K.; et al. Atomic layer deposition of zinc oxide on microrough zirconia to enhance osteogenesis and antibiosis. *Ceram. Int.* **2019**, *45*, 24757–24767. [CrossRef]

29. Skoog, S.A.; Elam, J.W.; Narayan, R.J. Atomic layer deposition: Medical and biological applications. *Int. Mater. Rev.* **2013**, *58*, 113–129. [CrossRef]

30. Falcó, I.; Randazzo, W.; Gómez-Mascaraque, L.G.; Aznar, R.; López-Rubio, A.; Sánchez, G. Fostering the antiviral activity of green tea extract for sanitizing purposes through controlled storage conditions. *Food Control* **2018**, *84*, 485–492. [CrossRef]

31. López de Dicastillo, C.; Patiño, C.; Galotto, M.J.; Palma, J.L.; Alburquenque, D.; Escrig, J. Novel antimicrobial titanium dioxide nanotubes obtained through a combination of atomic layer deposition and electrospinning technologies. *Nanomaterials* **2018**, *8*, 128. [CrossRef]

32. Park, J.Y.; Choi, S.W.; Kim, S.S. A synthesis and sensing application of hollow ZnO nanofibers with uniform wall thicknesses grown using polymer templates. *Nanotechnology* **2010**, *21*. [CrossRef]

33. Emamifar, A.; Kadivar, M.; Shahedi, M.; Soleimanian-Zad, S. Evaluation of nanocomposite packaging containing Ag and ZnO on shelf life of fresh orange juice. *Innov. Food Sci. Emerg. Technol.* **2010**, *11*, 742–748. [CrossRef]

34. Fang, X.; Li, S.; Wang, X.; Fang, F.; Chu, X.; Wei, Z.; Li, J.; Chen, X.; Wang, F. The growth and photocatalytic property of ZnO nanofibers synthesized by atom layer deposition using PVP nanofibers as templates. *Appl. Surf. Sci.* **2012**, *263*, 14–17. [CrossRef]

35. Guerrini, L.M.; de Oliveira, M.P.; Branciforti, M.C.; Custódio, T.A.; Bretas, R.E.S. Thermal and structural characterization of nanofibers of poly(vinyl alcohol) produced by electrospinning. *J. Appl. Polym. Sci.* **2009**, *112*, 1680–1687. [CrossRef]

36. Mallakpour, S.; Sadeghzadeh, R. Surface modification of alumina with biosafe molecules: Nanostructure, thermal, and mechanical properties of PVA nanocomposites. *J. Appl. Polym. Sci.* **2017**, *134*. [CrossRef]

37. Arun Kumar, N.B.; Sirajudeen, J.; Nagaswarupa, H.P.; Anil Kumar, M.R.; Ravi Kumar, C.R.; Gurushantha, K.; Shashi Shekhar, T.R.; Anantharaju, K.S.; Vishnu Mahesh, K.R.; Sharma, S.C.; et al. Photocatalytic and Photoluminescence studies of ZnO nanomaterials by Banana peel powder. In *Materials Today: Proceedings*; Elsevier Ltd.: Amsterdam, The Netherlands, 2017; Volume 4, pp. 11827–11836.

38. López de Dicastillo, C.; Roa, K.; Garrido, L.; Pereira, A.; Galotto, M. Novel polyvinyl alcohol/starch electrospun fibers as a strategy to disperse cellulose nanocrystals into poly(lactic acid). *Polymers* **2017**, *9*, 117. [CrossRef]

39. López de Dicastillo, C.; Garrido, L.; Alvarado, N.; Romero, J.; Palma, J.; Galotto, M. Improvement of polylactide properties through cellulose nanocrystals embedded in poly(vinyl alcohol) electrospun nanofibers. *Nanomaterials* **2017**, *7*, 106. [CrossRef]

40. Kayaci, F.; Ozgit-Akgun, C.; Donmez, I.; Biyikli, N.; Uyar, T. Polymer–inorganic core–shell nanofibers by electrospinning and atomic layer deposition: Flexible nylon–ZnO core–shell nanofiber mats and their photocatalytic activity. *ACS Appl. Mater. Interfaces* **2012**, *4*, 6185–6194. [CrossRef]

41. Velásquez, E.; Rojas, A.; Piña, C.; Galotto, M.J.; López de Dicastillo, C. Development of bilayer biodegradable composites containing cellulose nanocrystals with antioxidant properties. *Polymers* **2019**, *11*, 1945. [CrossRef]

42. Panea, B.; Ripoll, G.; González, J.; Fernández-Cuello, Á.; Albertí, P. Effect of nanocomposite packaging containing different proportions of ZnO and Ag on chicken breast meat quality. *J. Food Eng.* **2014**, *123*, 104–112. [CrossRef]

43. Zhang, L.; Ding, Y.; Povey, M.; York, D. ZnO nanofluids-A potential antibacterial agent. *Prog. Nat. Sci.* **2008**, *18*, 939–944. [CrossRef]

44. Kasemets, K.; Ivask, A.; Dubourguier, H.C.; Kahru, A. Toxicity of nanoparticles of ZnO, CuO and TiO2 to yeast Saccharomyces cerevisiae. *Toxicol. Vitr.* **2009**, *23*, 1116–1122. [CrossRef] [PubMed]

45. Karami, A.; Xie, Z.; Zhang, J.; Kabir, M.S.; Munroe, P.; Kidd, S.; Zhang, H. Insights into the antimicrobial mechanism of Ag and I incorporated ZnO nanoparticle derivatives under visible light. *Mater. Sci. Eng. C* **2019**, 107. [CrossRef] [PubMed]

46. López de Dicastillo, C.; Patiño, C.; Galotto, M.J.; Vásquez-Martínez, Y.; Torrent, C.; Alburquenque, D.; Pereira, A.; Escrig, J. Novel hollow titanium dioxide nanospheres with antimicrobial activity against resistant bacteria. *Beilstein J. Nanotechnol.* **2019**, *10*, 1716–1725. [CrossRef] [PubMed]

47. Azizi-Lalabadi, M.; Ehsani, A.; Divband, B.; Alizadeh-Sani, M. Antimicrobial activity of titanium dioxide and zinc oxide nanoparticles supported in 4A zeolite and evaluation the morphological characteristic. *Sci. Rep.* **2019**, *9*, 1–10. [CrossRef] [PubMed]

48. Bright, K.R.; Sicairos-Ruelas, E.E.; Gundy, P.M.; Gerba, C.P. Assessment of the antiviral properties of zeolites containing metal ions. *Food Environ. Virol.* **2009**, *1*, 37–41. [CrossRef]

49. Martínez-Abad, A.; Ocio, M.J.; Lagarón, J.M.; Sánchez, G. Evaluation of silver-infused polylactide films for inactivation of Salmonella and feline calicivirus in vitro and on fresh-cut vegetables. *Int. J. Food Microbiol.* **2013**, *162*, 89–94. [CrossRef]

50. Park, H.H.; Park, S.; Ko, G.; Woo, K. Magnetic hybrid colloids decorated with Ag nanoparticles bite away bacteria and chemisorb viruses. *J. Mater. Chem. B* **2013**, *1*, 2701–2709. [CrossRef]

51. Park, S.Y.; Park, H.H.; Kim, S.Y.; Kim, S.J.; Woo, K.; Ko, G. Antiviral properties of silver nanoparticles on a magnetic hybrid colloid. *Appl. Environ. Microbiol.* **2014**, *80*, 2343–2350. [CrossRef]

52. Castro-Mayorga, J.L.; Randazzo, W.; Fabra, M.J.; Lagaron, J.M.; Aznar, R.; Sánchez, G. Antiviral properties of silver nanoparticles against norovirus surrogates and their efficacy in coated polyhydroxyalkanoates systems. *LWT Food Sci. Technol.* **2017**, *79*, 503–510. [CrossRef]